A model-data comparison of $\delta^{13}C$ in the glacial Atlantic Ocean

T. Hesse,[1] M. Butzin,[1,2] T. Bickert,[2] and G. Lohmann[1]

Received 24 November 2010; revised 31 May 2011; accepted 13 June 2011; published 10 September 2011.

[1] We compare a compilation of 220 sediment core $\delta^{13}C$ data from the glacial Atlantic Ocean with three-dimensional ocean circulation simulations including a marine carbon cycle model. The carbon cycle model employs circulation fields which were derived from previous climate simulations. All sediment data have been thoroughly quality controlled, focusing on epibenthic foraminiferal species (such as *Cibicidoides wuellerstorfi* or *Planulina ariminensis*) to improve the comparability of model and sediment core carbon isotopes. The model captures the general $\delta^{13}C$ pattern indicated by present-day water column data and Late Holocene sediment cores but underestimates intermediate and deep water values in the South Atlantic. The best agreement with glacial reconstructions is obtained for a model scenario with an altered freshwater balance in the Southern Ocean that mimics enhanced northward sea ice export and melting away from the zone of sea ice production. This results in a shoaled and weakened North Atlantic Deep Water flow and intensified Antarctic Bottom Water export, hence confirming previous reconstructions from paleoproxy records. Moreover, the modeled abyssal ocean is very cold and very saline, which is in line with other proxy data evidence.

Citation: Hesse, T., M. Butzin, T. Bickert, and G. Lohmann (2011), A model-data comparison of $\delta^{13}C$ in the glacial Atlantic Ocean, *Paleoceanography*, *26*, PA3220, doi:10.1029/2010PA002085.

1. Introduction

[2] The state of deep water formation during the Last Glacial Maximum (LGM) has been debated by many and was reviewed recently [*Lynch-Stieglitz et al.*, 2007]. Based on proxy data many authors have suggested that the formation rate of North Atlantic Deep Water (NADW) was reduced during the LGM. This resulted in a shallower flow path of what is called Glacial North Atlantic Intermediate Water (GNAIW) [*Duplessy et al.*, 1988; *Curry and Oppo*, 2005; *Lynch-Stieglitz et al.*, 2007]. At the same time export of Antarctic Bottom Water (AABW) from the Southern Ocean intensified [*Ledbetter and Johnson*, 1976; *Robinson et al.*, 2005; *Negre et al.*, 2010]. Coupled ocean-atmosphere model simulations of the LGM climate show a large spread. *Otto-Bliesner et al.* [2007] found large variations in the glacial circulation produced by four different coupled models, while the same models produced similar circulations for the present day. *Weber et al.* [2007] compared the response of the Atlantic Meridional Overturning Circulation (AMOC) to LGM forcing in nine coupled models and found that model results differ widely. Coupled models even disagree as to whether the AMOC should have decreased or increased relative to the present day [*Hewitt et al.*, 2003; *Meissner et al.*, 2003; *Shin et al.*, 2003a; *Roche et al.*, 2007].

[3] The objective of this paper is to test in numerical sensitivity experiments which AMOC scenario could be reconciled with observed modern and past $\delta^{13}C$ distributions in the Atlantic Ocean, and to infer the climatic conditions and processes acting in the Atlantic Ocean during the LGM. For doing so, we compare three different LGM model circulation scenarios with a $\delta^{13}C$ data set of 220 sediment cores.

[4] Model-data comparisons are ultimately the best tool for testing competing forward modeling scenarios. There are but a few attempts to directly model marine proxy data for the LGM deep ocean. *Butzin et al.* [2005] looked at radiocarbon in the glacial ocean simulated by different model scenarios. As radiocarbon measurements are relatively sparse, however, it is difficult to constrain simulations and the real LGM ocean. Therefore, we are using the more widely distributed paleoproxy $\delta^{13}C$. *Winguth et al.* [1999] took a similar approach using ad hoc circulation fields and a limited amount of observations. Our data set of 220 $\delta^{13}C$ sediment cores in the entire Atlantic Ocean is unprecedented. Previous data compilations were restricted to particular Atlantic subareas, e.g., the western Atlantic [*Curry and Oppo*, 2005], the East Atlantic [*Sarnthein et al.*, 1994], or the South Atlantic [*Bickert and Mackensen*, 2004].

[5] The paper is structured in three parts. First, we assess the quality of the sediment cores used in this study. Second, we describe the model and its scenarios, and third, we compare the sediment data with the different scenarios.

2. Methods

[6] If calcareous $\delta^{13}C$ values of epibenthic foraminifera such as *Cibicidoides wuellerstorfi* ($\delta^{13}C_{foram}$) preserve the

[1]Alfred Wegener Institute for Polar and Marine Research, Bremerhaven, Germany.
[2]MARUM–Center for Marine Environmental Sciences, Bremen, Germany.

0883-8305/11/2010PA002085

$\delta^{13}C$ of Dissolved Inorganic Carbon (DIC) of the surrounding water ($\delta^{13}C_{DIC}$), we should be able to reconstruct past water mass geometries by looking at foraminiferal tests. This assumption has been shown to be true for most cases [*Woodruff et al.*, 1980; *Zahn et al.*, 1986; *Duplessy et al.*, 1988; *Hodell et al.*, 2001; *Mackensen*, 2008], but there are exceptions. *Mackensen et al.* [1993] showed that the $\delta^{13}C_{foram}$ value of *C. wuellerstorfi* can be significantly lower than the $\delta^{13}C_{DIC}$ of the surrounding water mass if the foraminifera feed on a phytodetritus layer that is derived from algal blooms at the surface. In section 2.2 we show that present-day measurements of $\delta^{13}C_{DIC}$ compare well with Late Holocene (LH) $\delta^{13}C_{foram}$.

2.1. Sediment Data

[7] We combined carbon isotope data from various compilations (*Sarnthein et al.* [1994], *Bickert and Mackensen* [2004], *Curry and Oppo* [2005], *Marchal and Curry* [2008]), and from the PANGAEA and NCDC databases (http://www.pangaea.de and http://www.ncdc.noaa.gov/paleo). As far as possible the original authors within the compilations were traced back and referenced. We only considered sediment cores containing *C. wuellerstorfi* which is known to be the most reliable conserver of $\delta^{13}C_{DIC}$ in the ocean [*Woodruff et al.*, 1980; *Belanger et al.*, 1981; *Zahn et al.*, 1986; *Hodell et al.*, 2001]. Some cores include a few other benthic species (*Planulina ariminensis* or *C. kullenbergi*), which are also used in this study, as they are thought to have an epibenthic habitat, too [*Lutze and Thiel*, 1989].

[8] For each core we calculated the average $\delta^{13}C$ value of the LH and LGM time slice (see below). Phytodetritus corrections like those used by *Bickert and Mackensen* [2004] were not applied to any of the data. We corrected the depth at which sediment cores were drilled by 120 meters in order to account for changes in sea level at the LGM [*Fairbanks*, 1989]. The table is available in the auxiliary material and at doi:10.1594/PANGAEA.758334.[1]

[9] To test whether $\delta^{13}C_{DIC} = \delta^{13}C_{foram}$ we used sediments from the LH (0–4 ka BP). Although there is evidence for variations in $\delta^{13}C$ during the Holocene period [*Oppo et al.*, 2003], our LH data set compares well with $\delta^{13}C_{DIC}$ measurements taken from GEOSECS and collected in GLODAP. Calculations on a subset of 58 cores in this period yielded an average standard deviation of $\delta^{13}C$ of 0.16‰ PDB (see section 2.2 below).

[10] Our definition of the LGM extends from 18–24 ka. Previously, authors have used different time constraints for the LGM, e.g., *Curry and Oppo* [2005] considered data from 18 to 21 ka BP (following the maximum positive peak in $\delta^{18}O$), whereas *Bickert and Mackensen* [2004] used the time interval from 19–23 ka BP (i.e., the glacial sea level lowstand [*Mix et al.*, 2001]). Other authors extended this range even further to 24 ka [*Ninnemann and Charles*, 2002] or 26.5 ka [*Clark et al.*, 2009]. Calculations on a subset of 64 cores (from PANGAEA) show that the average standard deviation of $\delta^{13}C$ within the cores used is 0.15‰ PDB for the 18–24 ka range. Since this only represents a minor $\delta^{13}C$ variation during the LGM we believe that our definition is justified. Age models for each core were taken from the original investigator(s).

2.2. Comparison of $\delta^{13}C_{DIC}$ Data and Late Holocene Sediment Data

[11] In order to estimate the uncertainty in LH $\delta^{13}C_{foram}$ values, we considered the $\delta^{13}C_{DIC}$ values as compiled by *Kroopnick* [1985] and measurements by P. Quay (University of Washington, collected in the GLODAP v1.1 bottle data set [*Key et al.*, 2004; *Sabine et al.*, 2005]). We calculated the Root Mean Square (RMS) difference between each DIC measurement which falls within a box of 500 km (meridionally) by 750 km (zonally) horizontally, by 250 m depth away from a sediment core measurement. These limits maximize the amount of data points, while at the same time ensuring reasonable oceanographic boundaries. The average RMS differences for the remaining 173 (GLODAP) and 200 (GEOSECS) measurements are 0.15 and 0.18‰ PDB, respectively.

[12] Figure 1 shows GLODAP $\delta^{13}C$ bottle data overlaying control run $\delta^{13}C$ as well as the $\delta^{13}C$ difference between control run and both, GLODAP data, and LH foraminifera. Model $\delta^{13}C$ values in the surface ocean and in the North Atlantic are higher compared to GLODAP. The control run underestimates the DIC measurements at intermediate depths around 1000 meters in the South Atlantic. This discrepancy will be addressed in detail below (see section 4.1).

2.3. Model Description

[13] The distribution of $\delta^{13}C$ in the glacial ocean is simulated using the marine carbon cycle model HAMOCC2s [*Heinze and Maier-Reimer*, 1999; *Heinze et al.*, 1999]. The model considers the dissociation of carbonic acid and the borate buffer as well as particulate organic carbon, calcium carbonate, and opal. In addition, HAMOCC2s includes a 10-layer sediment module (following *Archer et al.* [1993]) which accounts for chemical reactions of biogenic particulate matter with pore waters, diffusive processes in pore and bottom waters, vertical sediment advection as well as sediment accumulation, and bioturbation. Input of terrigenous matter is prescribed by present-day dust deposition [*Andersen et al.*, 1998] and by global-mean, present-day weathering fluxes at the sea surface, which are asymptotically approached by the integrated sediment accumulation during the model run. There is no iron limitation in HAMOCC2s. The model is able to diagnose atmospheric carbon dioxide (CO_2) as affected by processes in the ocean and yields a preindustrial concentration of 283 ppmV for $^{12}CO_2$. We do not attempt to capture the carbon-isotopic response to glacial-interglacial carbon cycle changes (e.g., in the terrestrial carbon pool, ocean alkalinity or the biological pump) but seek to investigate the isolated effect of various glacial ocean overturning scenarios on marine $\delta^{13}C$. For this reason all glacial model runs employ identical biogeochemical parameter settings for the preindustrial time.

[14] HAMOCC2s is driven by annual-mean thermohaline circulation fields provided by the Large Scale Geostrophic (LSG) Ocean General Circulation Model (OGCM), which are used 'off-line,' i.e., the fields are used for tracer advection without further dynamic computations (see *England and Maier-Reimer* [2001] for a review of tracer modeling). HAMOCC2s adopts the spatial resolution of the OGCM, but uses a different time step of one year. A parametrization

[1] Auxiliary materials are available in the HTML. doi:10.1029/2010PA002085.

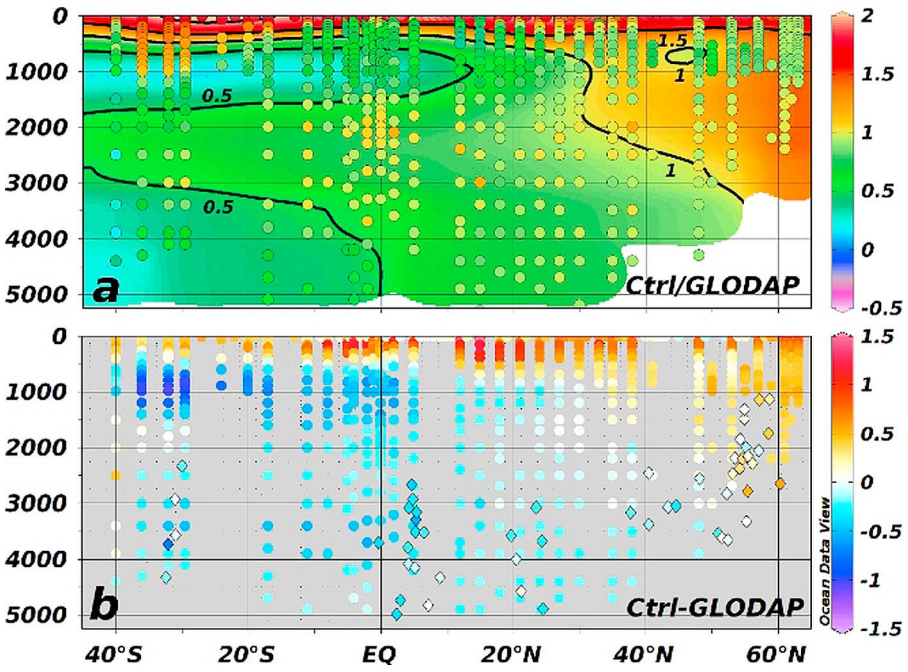

Figure 1. (a) Control run with GLODAP $\delta^{13}C_{DIC}$ bottle data overlay along the WHP A16 section and (b) the difference in $\delta^{13}C$ between the control run and both, GLODAP $\delta^{13}C_{DIC}$ (circles), and Late Holocene $\delta^{13}C_{foram}$ values (diamonds).

for convective mixing retains seasonality effects which would get lost otherwise [*Heinze and Maier-Reimer*, 1999]. The total integration time for the experiments is 70,000–100,000 years.

[15] We employ an updated version of the LSG ocean circulation model [*Maier-Reimer et al.*, 1993]. Our version includes a third-order advection scheme for tracers [*Schäfer-Neth and Paul*, 2001; *Prange et al.*, 2003] as well as an overflow parametrization for the bottom boundary layer [*Lohmann*, 1998; *Lohmann and Schulz*, 2000]. The setup is described in further detail by *Butzin et al.* [2005]. Model resolution is 3.5° on an Arakawa-E grid in the horizontal and 22 levels in the vertical. The LSG model is calibrated in simulations of $\Delta^{14}C$ [*Butzin et al.*, 2005]. The ocean is driven by 10-year-averaged monthly fields of wind stress, surface air temperature, and freshwater flux which will be discussed below. A surface heat flux formulation based on an atmospheric energy balance model permits that Sea Surface Temperatures (SSTs) can freely adjust to ocean circulation changes [*Rahmstorf and Willebrand*, 1995; *Prange et al.*, 2003; *Butzin et al.*, 2005]. The hydrological cycle is closed by a runoff scheme which allows that Sea Surface Salinities (SSSs) can freely evolve. The model uses an implicit method for the integration of the momentum equations with a time step of one month, and it is integrated over 20,000 years to quasi steady state conditions.

[16] The forcing fields for the LSG are derived in simulations using the atmospheric circulation model ECHAM3/T42 (carried out by *Lohmann and Lorenz* [2000] and *Prange et al.* [2004]), which by itself is forced with prescribed values of glacial insolation, CO_2, ice sheet cover and SSTs. We employ two different reconstructed glacial SST fields for which we make two experiments each. The first SST field is based on the CLIMAP reconstruction [*CLIMAP Project Members*, 1981] with an additional cooling of 3°C in the tropics between 30°N and 30°S [*Lohmann and Lorenz*, 2000], which is used for scenarios CB (CLIMAP Basic glacial) and CS (CLIMAP Southern Ocean freshwater changes). The second SST field is taken from the Glacial Atlantic Ocean Mapping (GLAMAP) reconstruction [see *Sarnthein et al.*, 2003, and references therein] in the globally extended version of *Paul and Schäfer-Neth* [2003], which is used for scenarios GB (GLAMAP Basic glacial) and GS (GLAMAP Southern Ocean freshwater changes). Compared to CLIMAP, GLAMAP SSTs are higher in the North Atlantic but lower in the tropical and South Atlantic. Correspondingly, GLAMAP suggests ice-free Nordic Seas in the summer and a winter sea ice margin similar to the CLIMAP sea ice boundary for summer. In the Southern Ocean, GLAMAP proposes more winter sea ice in Drake Passage, but less sea ice at the northern boundary of the Weddell Sea. In addition to the atmospheric forcing provided by ECHAM3, scenarios CS and GS feature a modified freshwater balance of the Southern Ocean which mimics additional brine release due to enhanced northward sea ice export, as suggested by recent LGM climate modeling studies [*Shin et al.*, 2003b; *Schmittner*, 2003]. This results in a very cold and very saline abyssal Atlantic which is depleted in $\Delta^{14}C$ [*Butzin et al.*, 2005], and improves the agreement with marine ^{14}C records and with other marine proxy data evidence for the LGM (*Adkins et al.* [2002]; see *Lynch-Stieglitz et al.* [2007] for a review). Experiment CB is not described further as temperature, salinity and radiocarbon distributions of this run are unrealistic [*Butzin et al.*, 2005].

2.4. Model-Data Comparison

[17] The model-data comparison was done in three steps: First, the control simulation was compared to LH data. For

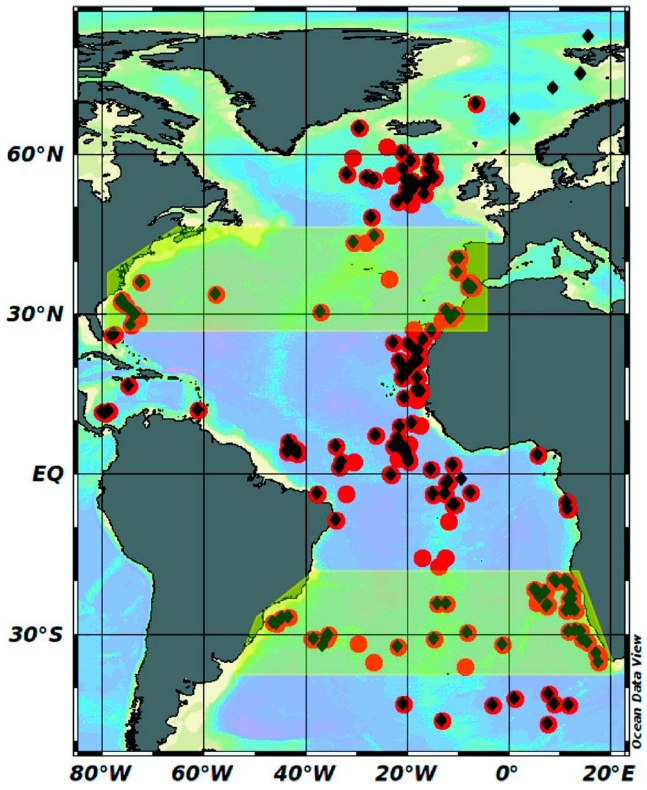

Figure 2. Sediment cores and section lines used in this study. Red dots (black diamonds) show core locations with Last Glacial Maximum (Late Holocene) $\delta^{13}C$ values. Meridional sections in the East and West Atlantic integrate data selected from east and west of the Mid-Atlantic Ridge, respectively. Zonal section lines and the area from which data are used in the North and South Atlantic are indicated in yellow (Figures S2 and S3 in the auxiliary material).

comparing the sediment data with the model output, we found the model grid point that is closest to a sediment core and compared the two $\delta^{13}C$ values. Cores that were not within 500 km (meridionally), 1100 km (zonally) and 500 m depth of a model grid point were removed from the comparison, leaving 201 cores. One model grid point may correspond to more than one sediment core. The spatial limits of the comparison were chosen, such that we could impose reasonable oceanographic boundaries while at the same time keeping a maximum number of sediment cores (note that the limits for the control run $\delta^{13}C$ to LH $\delta^{13}C_{foram}$ comparison are different from that of the present-day $\delta^{13}C_{DIC}$ to LH $\delta^{13}C_{foram}$ comparison). Second, we compared the absolute values of both, the LGM model runs and the LGM sediment data. Third, we looked at the $\delta^{13}C$ differences (anomalies, or $\Delta\delta^{13}C$) between our control run and the three glacial runs, and compared them to the difference between LH and LGM sediment data.

3. Results

[18] Results are presented along four sections. We consider two meridional sections, one in the East Atlantic, the other in the West Atlantic with the Mid-Atlantic Ridge being the dividing line (see Figure 2). Two zonal sections (see auxiliary material) run in the North Atlantic at approximately 37.5°N (the section line follows World Ocean Circulation Experiment Hydrographic Programme (WHP) section A3) and the South Atlantic at 30°S (WHP section A10).

3.1. Control Run

[19] The AMOC of our control run shows a maximum positive overturning strength of 16 Sv at a depth of 1 km between 20–50°N (Figure 3a). There is a sharp gradient in flow strength above the Greenland-Scotland Ridge at 67°N. Negative transport rates are associated with inflow of southerly-sourced water masses. CO_2 concentrations for the control run are at 283 ppmV.

[20] The control run shows three distinct $\delta^{13}C$ signatures in the Atlantic Ocean (see Figure 4): high $\delta^{13}C$ water extends from the North Atlantic into the South Atlantic down to 40°S, the main signal being at depths between 1.5–3.5 km. Low $\delta^{13}C$ water dominates the Southern Ocean and reaches as far north as the equator at a depth of 4 km. Another low $\delta^{13}C$ signature is observed at depths of around 1 km in the Southern Ocean, which extends northward to 20°N. The zonal section in the South Atlantic (see Figure S1 in the auxiliary material) shows that a relatively high $\delta^{13}C$ body dominates the western South Atlantic at a depth of 2.5 km, whereas in the eastern South Atlantic lower $\delta^{13}C$ water is more widespread.

[21] The difference plots between control run and LH sediment values (Figures 4 and S1) show that the control run yields lower $\delta^{13}C$ values than the sediment cores in most of the South Atlantic, but especially in the upper 2 km south of 20°S. There, the average difference is 0.52‰ PDB. In the North Atlantic model values are both, lower and higher than the sediment core $\delta^{13}C$. The difference, however, is small and rarely exceeds 0.2‰ PDB.

3.2. LGM Runs

[22] Presented are the results of the AMOC for the three LGM runs. Scenario CS shows a shoaled and weakened AMOC (see Figure 3b) compared to the control run. Maximum positive overturning is about 8 Sv at a depth of 500 m and between 20–40°N. In contrast, southerly-sourced waters are more widespread south of the equator at depths between 2–3 km. GB is characterized by strong, basin-filling transport of northerly-sourced waters (Figure 3c), with its maximum positive overturning (14 Sv) between 500–1000 m and 20–40°N. Negative overturning is only observed near the ocean floor and is nowhere stronger than 2 Sv. GS, finally, yields a shoaled positive AMOC cell with a maximum strength of 12 Sv centered between 400–900m and at 20–40°N. The upper 1.5 km of the ocean basin are in the positive AMOC regime. Negative overturning is slightly stronger (6 Sv) than for CS, and it extends further north. As already mentioned in section 2.3, HAMOCC2s can also diagnose atmospheric CO_2. The associated CO_2 concentrations (in ppmV) are 273 (GB), 244 (GS) and 225 (CS). The reduction is mostly due to increased formation of proto-AABW. It is beyond the scope of the paper, however, to discuss the CO_2 concentrations in more detail.

[23] All LGM runs show a similar large-scale pattern in the distribution of $\delta^{13}C_{DIC}$: the surface ocean contains the highest values, and the deep South Atlantic contains the lowest. CS shows the strongest meridional and vertical gradient in $\delta^{13}C$ values in the Atlantic Ocean (Figures 5 and 6).

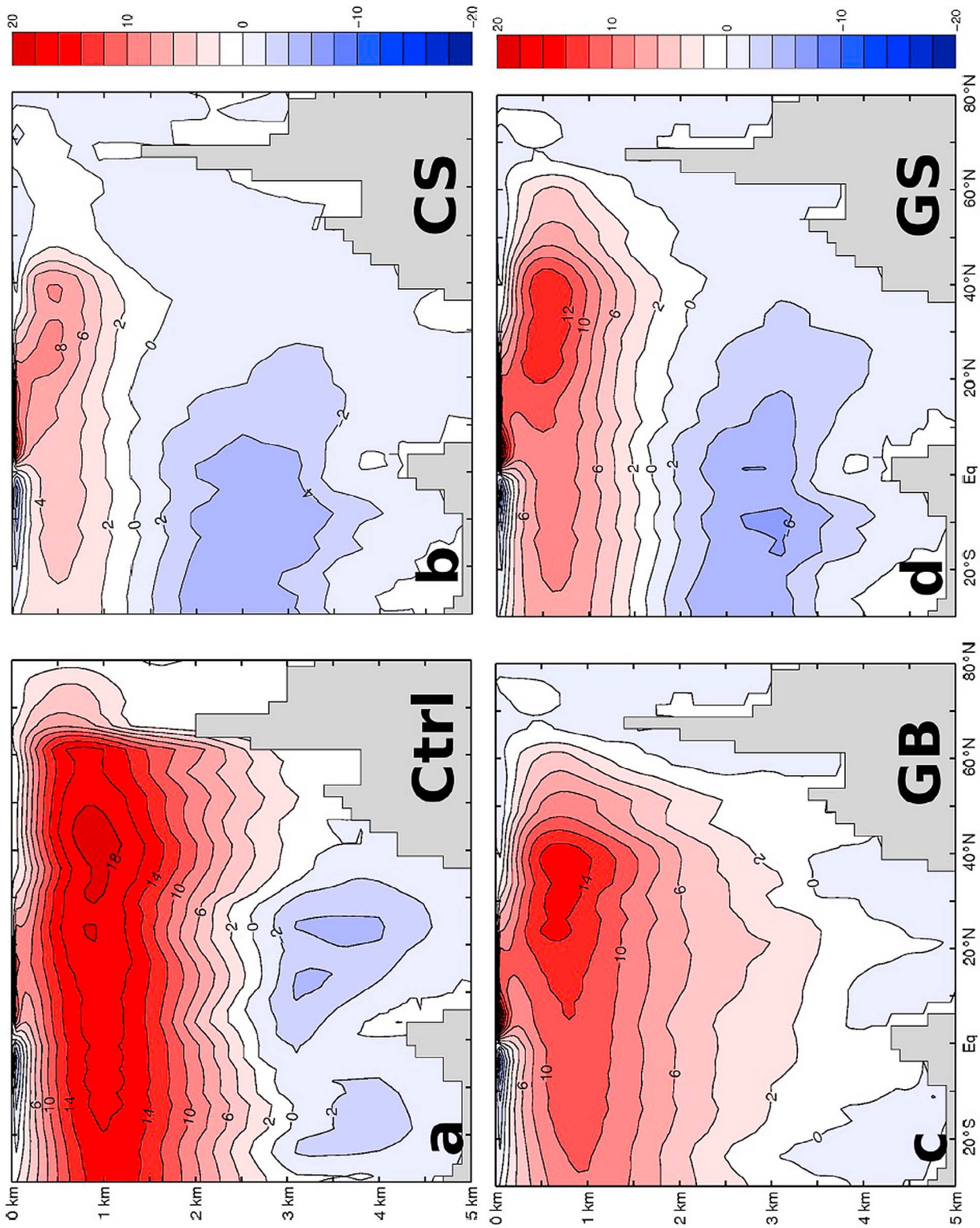

Figure 3. Meridional overturning circulation in the Atlantic Ocean (AMOC) for (a) the control run and (b, c, d) LGM runs CS, GB, and GS. Numbers are volume transport rates in *Sv* (10^6 m^{-3} s^{-1}).

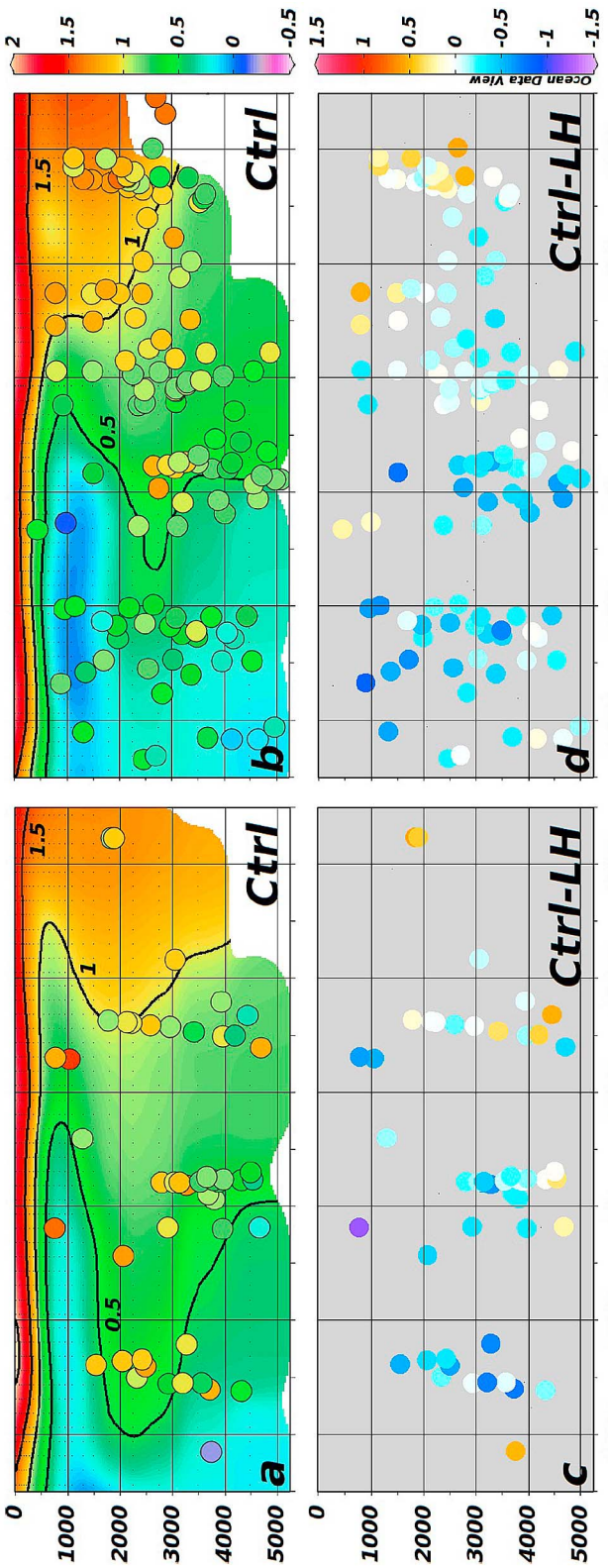

Figure 4. (a) Control run with Late Holocene $\delta^{13}C_{foram}$ data overlay for the West Atlantic and (c) the difference between control run $\delta^{13}C$ and Late Holocene $\delta^{13}C_{foram}$. (b, d) Like in Figures 4a and 4c but along the East Atlantic section. Positive numbers in Figures 4c and 4d indicate model $\delta^{13}C$ values that are higher than Late Holocene $\delta^{13}C_{foram}$ values.

In GS the gradient is reduced slightly, whereas in GB the $\delta^{13}C$ gradient is similar to that of the control run. All LGM runs show a prominent water body at intermediate depths in the southern East Atlantic with very low $\delta^{13}C$ values (from −0.4‰ PDB in GB to less than −0.5‰ PDB in CS, see Figure 5). All runs also show a more or less pronounced tongue of low $\delta^{13}C$ water at depths of 750–1000 m in the western South Atlantic (Figure 6 and Figure S3).

[24] In CS high $\delta^{13}C$ values (greater than 1‰ PDB) reach down to depths of 1.5 km in the eastern North Atlantic north of 40°N. For the western North Atlantic this high $\delta^{13}C$ body extends even further south to 20°N (Figure 6a). Conversely, low $\delta^{13}C$ (less than 0‰ PDB) dominates the deep western South Atlantic below depths of 3 km reaching as far north as 50°N, whereas in the eastern Atlantic, south of 10°N low $\delta^{13}C$ fills the entire ocean basin below 1 km water depth (see Figure S3a in the auxiliary material).

[25] In GB the entire North Atlantic north of 40°N is dominated by high $\delta^{13}C$, which extends south to 15°N in the western North Atlantic. Values of $\delta^{13}C$ below 0‰ PDB only exist in the western South Atlantic below 2 km water depth and south of 35–40°S, and in the intermediate eastern South Atlantic (Figure 5c).

[26] GS shows $\delta^{13}C$ values higher than 1‰ PDB in the North Atlantic in the upper 1.5 to 2 km extending south to 30°N in the eastern Atlantic, and to 10°N in the western Atlantic (compare Figures 5e and 6e). Low $\delta^{13}C$ values take up the western Atlantic below depths of 3 km reaching as far north as 8°N. Conversely, in the eastern Atlantic south of 8°N $\delta^{13}C$ is lower than 0‰ PDB everywhere except for the upper 1 km of the water column.

[27] The correlation coefficient r between $\delta^{13}C$ values of the three model runs and the glacial sediment core data is 0.72 for CS, 0.31 for GB, and 0.76 for GS. The RMS difference between model scenario and sediment data yields 0.70,1.06 and 0.68‰ PDB for CS, GB and GS, respectively. The Taylor diagram [*Taylor*, 2001] summarizes the correlation coefficients and centered RMS differences for different areas of the Atlantic Ocean (Figure 7).

[28] In the North, West, and East Atlantic $\delta^{13}C_{GS}$ correlates strongest with the sediment data (r = 0.82, 0.78, and 0.73, respectively). In the South Atlantic r is lower than 0.30 for all model scenarios. The GB correlation coefficient is nowhere greater than 0.35.

3.3. Anomalies or $\Delta\delta^{13}C$

[29] The $\Delta\delta^{13}C$ plot for the sediment data (Figure 8a) shows that the LH $\delta^{13}C$ data are more negative than the LGM data in the northern Atlantic at depths above 1.5 to 2 km, but are more positive in all areas below 2 km water depth. The $\delta^{13}C$ values in the top 2 km in the eastern South Atlantic are similar for the two time slices.

[30] The maximum positive anomaly for GB is in the central Atlantic Ocean between 40°N and 40°S and depths between 500 m and 2500 m (up to 0.5‰ PDB). Negative anomalies (values of −0.3‰ PDB) are present in the tropical and North Atlantic surface ocean as well as at depths below 3 km north of 20°S.

[31] CS anomalies are most negative in the upper 1250 m of the North Atlantic (−0.6‰ PDB), but positive below 1500 m water depth. Positive anomalies are strongest in the deep North Atlantic (up to +1‰ PDB), whereas they are weaker in the deep South Atlantic (+0.5‰ PDB). Anomalies are zero south of 40°S at depths above 1.5 km.

[32] GS anomalies are similar in magnitude to CS anomalies, but less pronounced: negative anomalies in the North Atlantic above depths of 1500 m and in the tropical surface ocean, and positive anomalies in most of the remaining ocean basin. Maximum positive values are found in the deep North Atlantic and the middepth tropical Atlantic (+0.7‰ PDB), lower ones in the deep South Atlantic (+0.4‰ PDB).

4. Discussion

4.1. Control Run

[33] The control run captures the general $\delta^{13}C$ features observed in the water column of the present-day Atlantic and in LH sediment cores. Compared to GLODAP, control run $\delta^{13}C$ values are higher in the North Atlantic. This is most likely explained by the Suess effect, which has recently been shown to penetrate down to 2500 meters depth and southwards to 30°N in the North Atlantic [*Olsen and Ninnemann*, 2010]. Two cores near the Bahamas by *Slowey and Curry* [1995], OCE205-33GGC and OCE205-100GGC, have higher $\delta^{13}C$ values than are seen in the control run. GLODAP $\delta^{13}C_{DIC}$ measurements, however, contradict such high $\delta^{13}C_{foram}$ values. The control run correlates very well with LH sediment data in the Northern Atlantic (see Figure 4), but underestimates the observations in some areas of the South Atlantic. Model $\delta^{13}C$ values in the upper 500–2000 m in the South Atlantic are lower than foraminiferal $\delta^{13}C$ by more than 0.5‰ PDB. This seems to be a general model problem, that is also present in the glacial model scenarios (see below).

[34] An altered Redfield stoichiometry for Southern Ocean and Antarctic surface and intermediate depth waters (as suggested by *Zahn and Keir* [1994] or *Lynch-Stieglitz et al.* [1995]) could be the source for the lower-than-observed Antarctic Intermediate Water (AAIW) $\delta^{13}C$ in the model. *Zahn and Keir* [1994] argued that isotopically depleted $CO_{2(aq)}$ readily enters the atmosphere once the upwelled waters come into contact with the sea surface. At the same time nutrients are not taken up by photosynthesis to such a degree that would ensure a constant Redfield stoichiometry, which in turn would lead to higher-than-expected $\delta^{13}C$ values for AAIW.

[35] Following *Broecker and Maier-Reimer* [1992] and *Lynch-Stieglitz et al.* [1995] we investigate the contribution of the air-sea exchange ($\delta^{13}C_{as}$) to the carbon isotopic composition of surface water by removing the biological component from the total modeled or observed $\delta^{13}C$ signal:

$$\delta^{13}C_{as} = \delta^{13}C - (2.7 - 1.1 \times PO_4),$$

where PO_4 is the phosphate concentration. Our control run yields positive values of $\delta^{13}C_{as}$ in the AAIW formation area, which indicates that the isotopic signature of our modeled AAIW is substantially influenced by isotopic air-sea fluxes (Figure S4). However, our model values of $\delta^{13}C_{as}$ (about 0.2‰ PDB) are significantly smaller than observations (of up to 1‰ PDB according to *Mackensen et al.* [1996]) which suggests that our carbon cycle model underestimates the isotopic air-sea exchange in the AAIW formation area. This is probably due to the air-sea exchange formulation in the

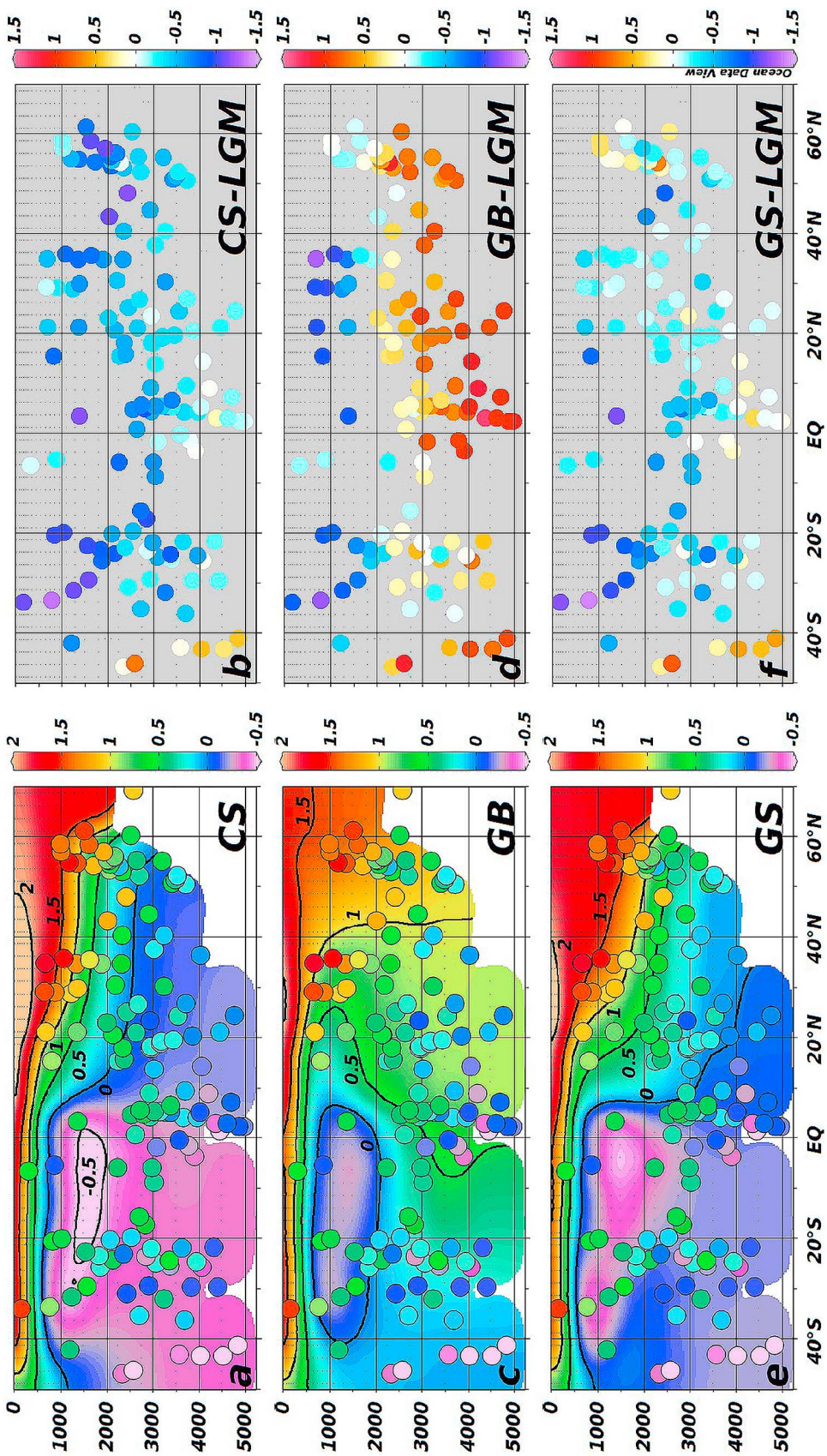

Figure 5. East Atlantic section: (a) CS $\delta^{13}C$ with LGM $\delta^{13}C_{foram}$ data overlay, and (b) model-data differences. In Figure 5b positive numbers indicate model $\delta^{13}C$ values that are higher than $\delta^{13}C_{foram}$ values. (c–f) Like in Figures 5a and 5b but for model runs GB (Figures 5c and 5d) and GS (Figures 5e and 5f).

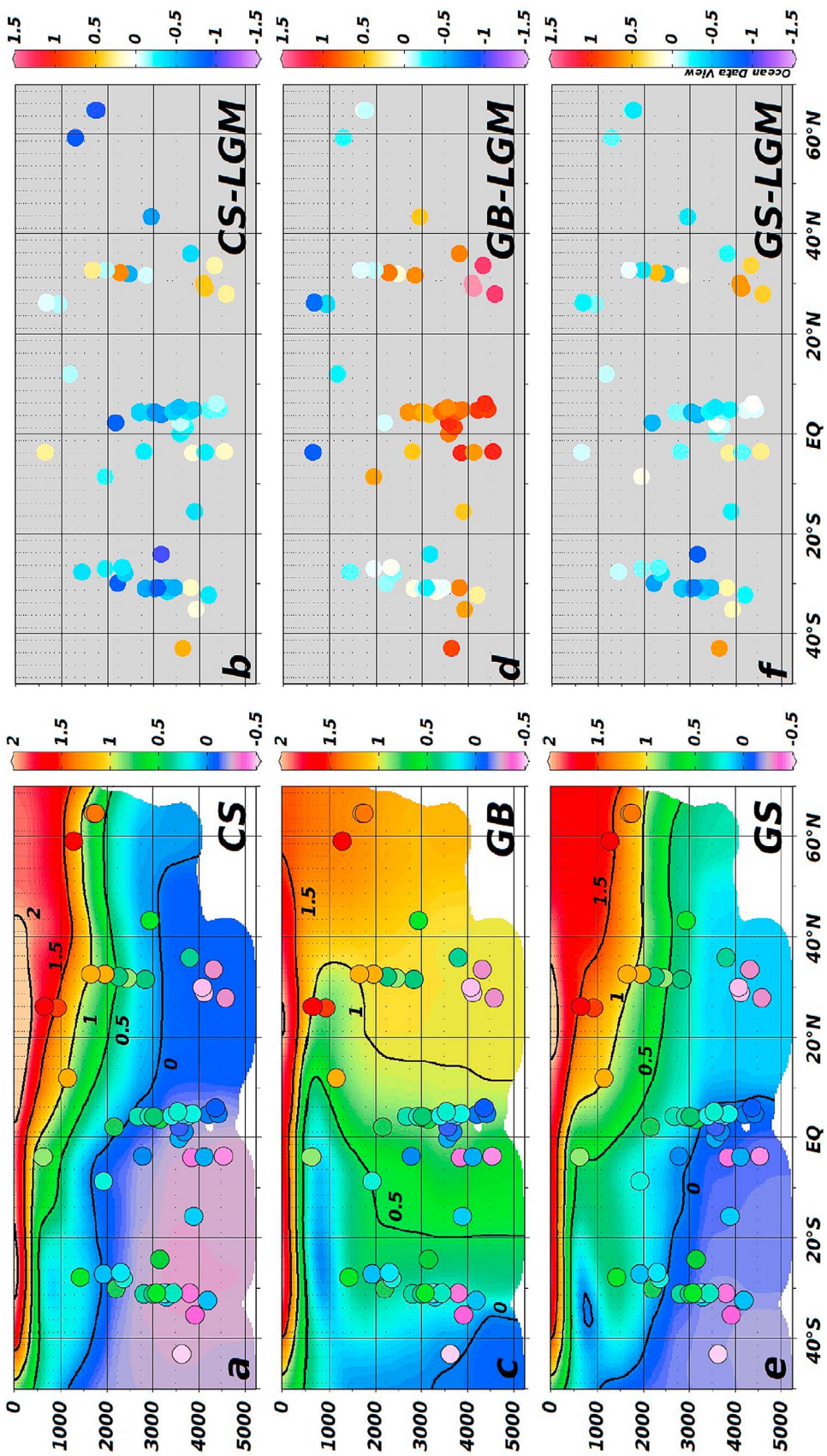

Figure 6. Like Figure 5, but along the West Atlantic section.

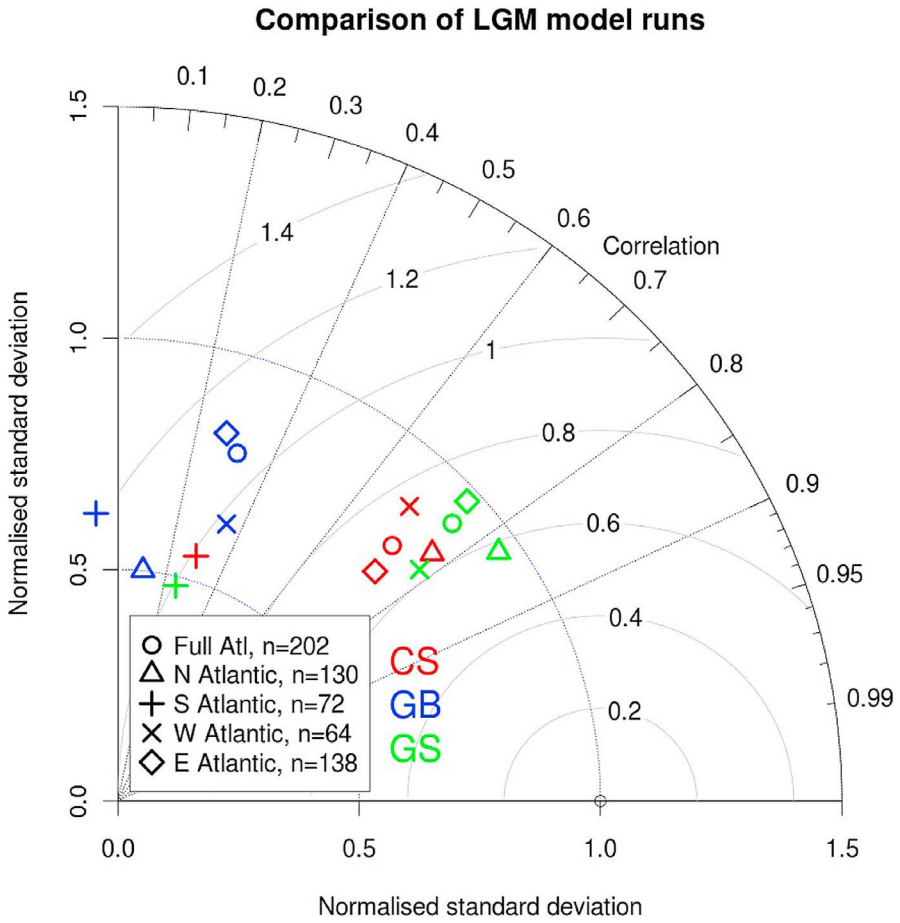

Figure 7. Taylor diagram [*Taylor*, 2001] showing the correlation coefficients (along the arc) and the centered RMS differences (gray solid arcs of circles) for the three LGM scenarios and different Atlantic regions when compared to the LGM $\delta^{13}C_{foram}$ data. The number of data points included in each subarea is given by *n*. The normalized standard deviation is a measure for $\delta^{13}C$ variance in the model with respect to the observations.

model which does not explicitly depend on the wind speed but employs a globally averaged gas transfer velocity value. This model deficit is also corroborated by the results from a numerical sensitivity study carried out by *Broecker and Maier-Reimer* [1992] who (employing an earlier version of our model) found that by doubling the air-sea exchange rate of CO_2 the $\delta^{13}C$ values in the formation region of AAIW would increase by 0.4‰ PDB.

4.2. LGM Runs

[36] The model-data difference plots (Figures 5 and 6) indicate that model results are systematically higher than observations in the deep South Atlantic and along the North American coast. In the deep Southern Ocean south of 40°S GS simulates $\delta^{13}C$ values that are higher by 0.23 to 0.84‰ PDB than a whole suite of sediment cores (PS1745-3 and PS2082-1 [*Mackensen et al.*, 1994], TTN057-6 [*Hodell et al.*, 2003], RC15-93, RC15-94, TN057-21 and V22-108 [*Ninnemann and Charles*, 2002], see Figures 5 and 6). The $\delta^{13}C$ values in the cores reported by *Ninnemann and Charles* [2002] are based on both *C. wuellerstorfi* and *C. mundulus*. *Hodell et al.* [2001] showed that *C. kullenbergi* (which is the same species as *C. mundulus* [*Yu et al.*, 2008]) records systematically lower $\delta^{13}C$ values than *C. wuellerstorfi*. Extrapolating the $\delta^{13}C_{kullenbergi}$ data scatter to −0.80‰ PDB suggests a $\delta^{13}C_{wuellerstorfi} \approx 0$‰ PDB [see *Hodell et al.*, 2001, Figure 1]. Some of the difference seen in the model-data comparison could therefore be taken up. Another possible influence is the phytodetritus effect [*Mackensen et al.*, 1993], which causes foraminifera to record lower-than-expected $\delta^{13}C$ values, typically explaining 0.4‰ PDB. Cores that lie close to an oceanic front are potentially affected. The coarse model resolution does not permit to capture steep oceanographic gradients such as oceanic fronts, which may also partly explain the model-data offset in the Southern Ocean. LGM reconstructions of oceanic fronts in the Southern Ocean by *Gersonde et al.* [2003, 2005] suggest that the Polar Front (PF), the Sub-Antarctic Front (SAF) and the Sub-tropical Front (STF) shifted northward by 3–5°. Careful comparison of the frontal positions with the locations of the relevant cores shows that PS1745-3 and RC15-93 fall exactly on the reconstructed PF, whereas PS2082-1 and TTN57-6 coincide with the reconstructed SAF. Cores RC15-94 and V22-108 fall in between the reconstructed PF and SAF, TN057-21 lies between the reconstructed SAF and STF. Since oceanic fronts meander about their mean position, the latter cores

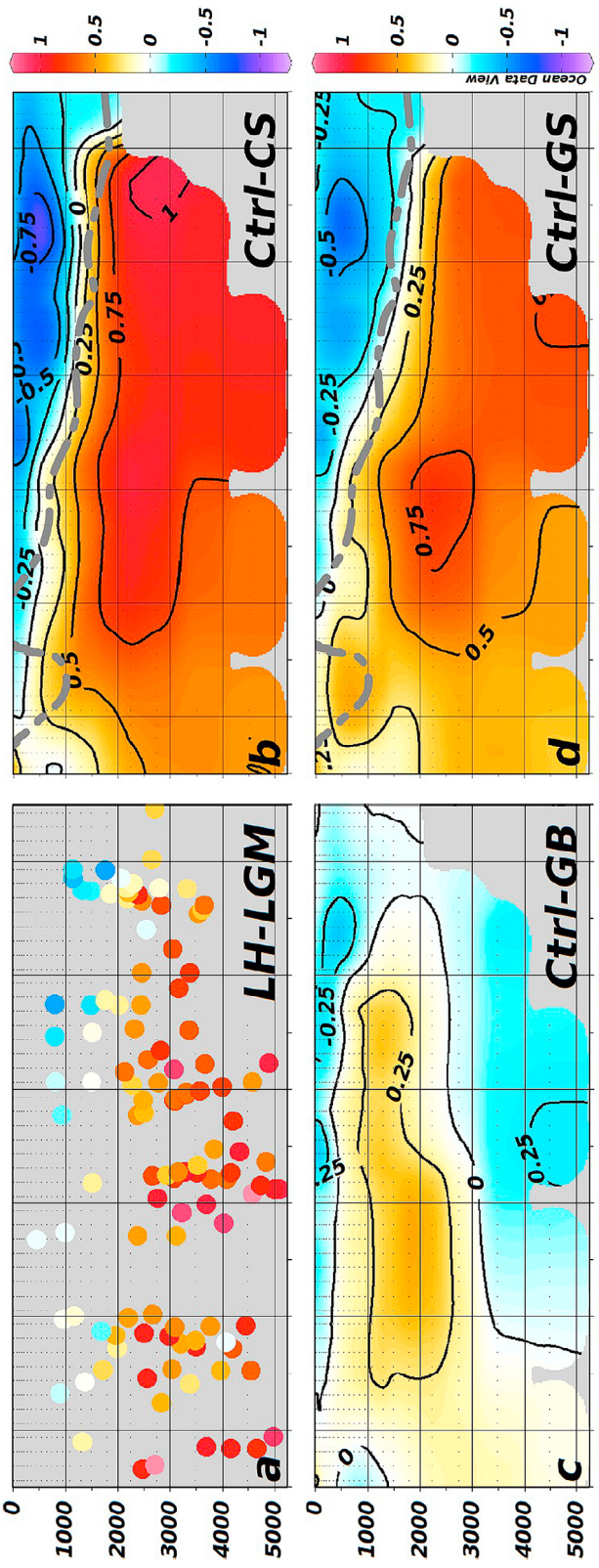

Figure 8. East Atlantic $\Delta\delta^{13}C$ plots (anomalies): (a) difference between LH and LGM sediment data and differences between control run and (b) CS, (c) GB, and (d) GS. Sediment data indicate a strong $\Delta\delta^{13}C$ gradient between the surface/intermediate ocean and the deep ocean. Gray dash-dotted lines in Figures 8b and 8d are zero-lines which are based on observations (Figure 8a).

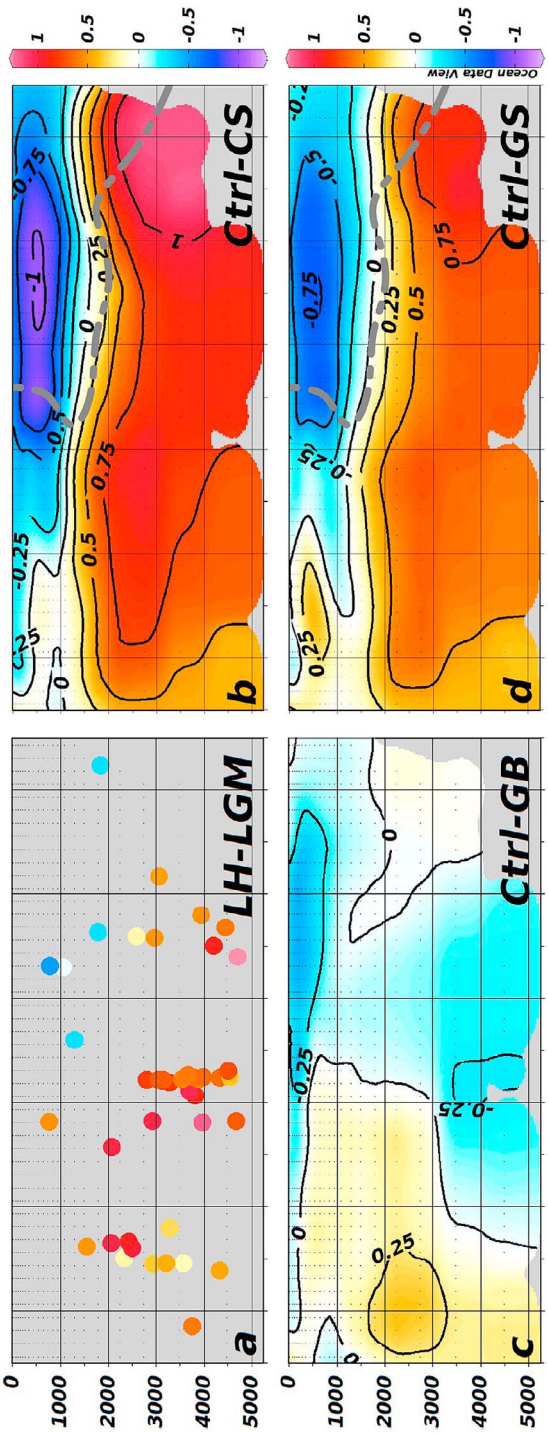

Figure 9. Like Figure 8, but along the West Atlantic section.

may also be affected by the phytodetritus effect. Hence, both factors, measurements on epibenthic species other than *C. wuellerstorfi* and changes in frontal positions with the associated phytodetritus effect, may explain model-data differences in the deep Southern Ocean.

[37] In the western North Atlantic below 4 km and between 20–30°N there are four cores which have δ^{13}C values that are lower than GS by 0.40 to 0.62‰ PDB (KNR140-12JPC, KNR140-22JPC and KNR140-28GGC [*Keigwin*, 2004], EN120-1GGC [*Boyle and Keigwin*, 1987], see Figure 6). The horizontal flow fields of model runs CS and GS (not shown) reveal an AABW influx in the deep western North Atlantic. The model δ^{13}C signal, however, is still too high. *Keigwin* [2004] stresses that measurements of Holocene δ^{13}C values in this location below 3 km do not agree with present-day DIC measurements, which may point toward yet unknown problems with these cores.

[38] There are also areas where model results indicate lower δ^{13}C values than observational δ^{13}C values. This is particularly true for the intermediate depth South East Atlantic, the Brazil margin cores, the central North Atlantic (see Figure S2), and the central South Atlantic at 3 km water depth.

[39] In the South East Atlantic all model scenarios (including the control run) yield lower δ^{13}C values by about −1‰ PDB compared to the sediment data (175-1087A [*Pierre et al.*, 2001], ODP1085A [*Bickert and Mackensen*, 2004], IOW226920-3 [*Mollenhauer et al.*, 2002], and KW-31 [*Sarnthein et al.*, 1994]). Sediment $\delta^{13}C_{foram}$ data are consistently higher than any model simulation δ^{13}C, and model results of temperature and salinity (not shown) do not point toward any anomalous water mass here. The low model δ^{13}C is likely to be an artefact which may partly be caused by underestimation of carbon isotope air-sea exchange in the formation region of AAIW (see control run discussion above). For the LGM scenarios this misrepresentation might be exacerbated due to generally stronger and seasonally more varying glacial winds, which may cause the anomalously low δ^{13}C signal in the South East Atlantic. One might also speculate about a Mediterranean influence: *Zahn et al.* [1987] find that Mediterranean Outflow Water (MOW) has a δ^{13}C signature that was higher during the LGM (greater than 1.6‰ PDB) when compared to today (1.3‰ PDB). *Bickert and Mackensen* [2004] show that MOW extends southwards after leaving the Strait of Gibraltar. It cannot be verified, however, that MOW extends further south than 10°N at depths above 2500 meters, as there are no sediment cores at these depths away from the continental slope. Moreover, the difference in MOW δ^{13}C between today and the LGM is small (0.3‰ PDB) compared to the difference seen in the model-data comparison in the middepth South East Atlantic (1‰ PDB). There is no Mediterranean in our LGM setup.

[40] Most of the Brazil margin cores of *Curry and Oppo* [2005] between 25–35°S contain δ^{13}C values that are higher by up to 0.60‰ PDB than model values in GS (e.g., CHN115-70PC, CHN115-89PC, or CHN115-91PC, see Figure 6f). The same data-model difference holds for the LH data and our control simulation (Figure 3c). The most likely culprit is again poor carbon isotope air-sea exchange in the model (see control run discussion above), which is likely to be more pronounced in our LGM runs. Additionally, upwelling of NADW-derived waters south of Cape Frio would introduce much higher δ^{13}C values [*Acha et al.*, 2004], but the model cannot resolve such local upwelling features.

[41] Several cores in the central North Atlantic between 25–40°W and at 2–3.5 km water depth are enriched in ^{13}C with respect to either GS or CS (e.g., CHN824115 [*Boyle and Keigwin*, 1987], or T86-15P [*Sarnthein et al.*, 1994]) with δ^{13}C values relative to GS that are higher by 0.42 to 0.66‰ PDB (see Figure S2). This points toward a model NADW flowpath that is too shallow in the central North Atlantic.

[42] Analogously, there are four cores in the central South Atlantic by *Bickert and Mackensen* [2004] for which scenario GS simulates δ^{13}C values that are lower than observations by 0.58 to 0.88‰ PDB (GeoB3808-6, GeoB5115-2, GeoB5121-2, and GeoB2016-1). Again, one may speculate about a NADW signal in the sediments that neither model scenario captures as model-NADW is shoaling too much. Additionally, the model problems seen in the South East Atlantic may contribute by extending into the central South Atlantic.

4.3. Anomalies or $\Delta\delta^{13}$C

[43] The $\Delta\delta^{13}$C plots in Figures 8 and 9 have the advantage that systematic errors such as constant offsets in δ^{13}C values in the sediments due to, e.g., upwelling, or model artefacts such as the one seen in the South East Atlantic, are reduced. Scenario GB performs poorly when compared to the sediment data (Figures 8a, 8c, 9a, and 9c). $\Delta\delta^{13}$C is similar in both CS and GS. For the sediments the $\Delta\delta^{13}C = 0$ line lies close to 2 km water depth. The same holds for GS, but not for CS, where the zero-line is above 1.4 km water depth (Figures 8b and 9b). In addition, the average sediment $\Delta\delta^{13}$C signal below 2 km water depth is less than 0.75‰ PDB, which is similar to GS. In CS this value is mostly above 0.75‰ PDB. This further strengthens the good agreement of scenario GS with the observations. The sediment cores south of 40°S are only affected by frontal upwelling during the LGM and not during the LH (see above). Therefore, the effect is not systematic, and the high $\Delta\delta^{13}$C in the sediments comes as no surprise.

[44] The differences between our three model scenarios are summarized in Figure 7. Scenarios GS and CS both correlate very well with the sediment data. GS, however, correlates better in the North, West and East Atlantic. Additionally, the variance in GS is closer to that of the reconstructions. Scenario GB performs poorly in the model-data comparison.

[45] The altered fresh water balance in the Southern Ocean which is employed in both, GS and CS, seems to be a crucial feature in our LGM simulations. It is caused by (1) enhanced northward sea ice export and melting away from the sea ice production zone, which in turn causes (2) a relative increase in brine rejection when new sea ice is forming. The overturning cell in the North Atlantic is shoaling and weakening for both scenarios, indicating another important LGM feature (Figure 3). The strength of the positive overturning cell, however, is less well constrained: 12 Sv for GS contrast with only 8 Sv for CS, although both scenarios show a good fit for the North Atlantic. This significant difference in the response of the model to the two different SST reconstructions deserves further explanation. It is important to note that the SST reconstructions have an impact on atmospheric wind patterns and evaporation/precipitation patterns that the atmospheric model generates,

which in turn have an impact on freshwater and heat fluxes into the ocean, ocean circulation, and air-sea gas exchange [see also *Romanova et al.*, 2004]. Scenario GS, for instance, has surface waters south of Iceland that are saltier by more than 2 PSU when compared to CS (not shown). This causes stronger downwelling and is very likely the reason for the more rigorous AMOC in scenario GS compared to CS. Since $\delta^{13}C$ is not a purely kinematical tracer, it can only be used to reconstruct the geometries of water masses. The strength of the overturning cell cannot be assessed.

4.4. Relation to Previous Studies

[46] Previous model-data comparisons have either used a much reduced number of observations, or not employed a 3D OGCM. *Winguth et al.* [1999] used ad hoc circulation fields and a limited amount of mostly East Atlantic observations. Their glacial first guess scenario yields a reduced North Atlantic overturning circulation, which is compensated for by an increased influx of Southern Ocean deep waters. This result is similar to what we find for scenario GS, but there are conceptual differences. *Winguth et al.* [1999] prescribed estimated salinity fields which were additionally modified in high latitudes to reduce the model-data misfit. In our model setup, salinity is a fully prognostic variable, which is physically more consistent.

[47] *Tagliabue et al.* [2009] employ an OGCM and a biogeochemistry model forced by different LGM boundary conditions. Their model scenario that agrees best with observations (CircA) has a reduced ventilation in the North Atlantic and reduced AABW export. Their increased AABW export scenario (CircB) does not agree well with observations. This is the opposite of what our $\delta^{13}C$ model results show: our two best fitting scenarios arrive at increased AABW export from the Southern Ocean. Since increased AABW inflow into the North Atlantic is also supported by radiocarbon, grain size, and Pa/Th studies [*Robinson et al.*, 2005; *Hall et al.*, 2011; *Negre et al.*, 2010] we believe that our GS and CS model scenarios are well suited to describe the LGM Atlantic Ocean state.

[48] So far most modeling studies have focused on changing the freshwater balance in the North Atlantic [*Roche et al.*, 2007; *Kageyama et al.*, 2009; *Otto-Bliesner and Brady*, 2010], with mixed successes regarding the integrity with observational data. Changes in freshwater production in the Southern Ocean [*Adkins et al.*, 2002] have attracted comparatively less attention, but seem to be important [*Stocker et al.*, 1992; *Fichefet et al.*, 1994; *Winguth et al.*, 1999; *Seidov et al.*, 2001; *Shin et al.*, 2003b; *Schmittner*, 2003; *Butzin et al.*, 2005]. *Schmittner* [2003] increased rates of sea ice formation and northward export while keeping the AMOC strength at present-day levels. This resulted in saltier and denser AABW, increased its formation rate, and led to a higher consistency with reconstructions of glacial bottom water properties. *Shin et al.* [2003a] modeled enhanced northward sea ice export in the Southern Ocean in a fully coupled ocean-atmosphere circulation model and arrived at a shoaled and weakened AMOC. *Butzin et al.* [2005] found that modeling radiocarbon in the glacial ocean with a changed freshwater balance in the Southern Ocean agrees best with observations. Our study with its widespread collection of $\delta^{13}C$ values puts these modeling efforts on a more comprehensive observational base and further highlights the Southern Ocean's role in influencing global glacial climate.

5. Conclusions

[49] The objective of this paper is to test in numerical sensitivity experiments which AMOC scenario could be reconciled with observed modern and past $\delta^{13}C$ distributions in the Atlantic Ocean, and to infer the climatic conditions and processes acting in the Atlantic Ocean during the LGM. We have assembled a $\delta^{13}C$ data set of 220 sediment cores that we compare to three different LGM model scenarios.

[50] The model scenario that best correlates with observations (r = 0.76) has a shoaled positive overturning circulation in the North Atlantic that is reduced by 40% compared to the present day. Northward AABW flux is intensified. This scenario (GS) is based on GLAMAP SSTs and employs an altered freshwater balance in the Southern Ocean that mimics increased sea ice export and melting at latitudes between 50–55°S, north of the sea ice production zone.

[51] GS correlates best in the northern (r = 0.82), western (0.78) and eastern Atlantic (0.73), with a $\delta^{13}C$ variance that is close to the observed $\delta^{13}C_{foram}$ variance. Scenario CS, which is forced by CLIMAP SSTs, also uses an altered freshwater balance in the Southern Ocean, and has a weak AMOC. It performs slightly worse than GS in all Atlantic subareas, and also with regard to the variance. Our glacial base scenario GB with its strong AMOC similar to the present day does not agree with observations.

[52] Some differences between model and sediment data $\delta^{13}C$ values can be explained by local effects (e.g., upwelling) and known model deficiencies. In particular, the poor representation of carbon isotope air-sea exchange in the AAIW formation region due to globally averaged wind fields in the carbon cycle model causes lower-than-observed $\delta^{13}C$ model values. An implementation of seasonally varying wind patterns in the carbon cycle model as well as higher model resolution in critical areas such as near oceanic fronts is therefore desirable.

[53] Our results further corroborate that the AMOC cell shoaled to less than 2000 meters water depth during glacial times. By how much the positive AMOC strength weakened cannot be established, because different boundary conditions and overturning strengths, as found in GS and CS, yield similar results for $\delta^{13}C$. GS with its more recent GLAMAP reconstruction shows an AMOC weakening to 12 Sv, which is a reduction by 40% compared to its present-day strength. The increased negative AMOC at depth in scenarios GS and CS is in line with and further supports recent Pa/Th and grain size studies [*Negre et al.*, 2010; *Hall et al.*, 2011]. Our findings further underline that the Southern Ocean's fresh water balance might play a key role in explaining the glacial ocean.

[54] **Acknowledgments.** We are grateful to Bill Curry for providing his Western Atlantic sediment core data. We thank Andreas Mackensen, Gregor Knorr, and Delia Oppo for useful discussions. Technical assistance was expertly provided by Andreas Manschke, Rainer Sieger, and Reiner Schlitzer. We also thank Rainer Zahn and two anonymous reviewers for helpful comments that substantially improved the manuscript. This research was supported by the Helmholtz Graduate School for Polar and Marine Research (POLMAR) and the ESF.

References

Acha, E. M., H. W. Mianzan, R. A. Guerrero, M. Favero, and J. Bava (2004), Marine fronts at the continental shelves of austral South America physical and ecological processes, *J. Mar. Syst.*, *44*(1–2), 83–105, doi:10.1016/j.jmarsys.2003.09.005.

Adkins, J. F., K. McIntyre, and D. P. Schrag (2002), The salinity, temperature, and $\delta^{18}O$ of the glacial deep ocean. *Science*, *298*(5599), 1769–1773, doi:10.1126/science.1076252.

Andersen, K. K., A. Armengaud, and C. Genthon (1998), Atmospheric dust under glacial and interglacial conditions, *Geophys. Res. Lett.*, *25*, 2281–2284, doi:10.1029/98GL51811.

Archer, D., M. Lyle, K. B. Rodgers, and P. Froelich (1993), What controls opal preservation in tropical deep-sea sediments?, *Paleoceanography*, *8*, 7–21, doi:10.1029/92PA02803.

Belanger, P. E., W. B. Curry, and R. K. Matthews (1981), Core-top evaluation of benthic foraminiferal isotopic ratios for paleo-oceanographic interpretations, *Palaeogeogr. Palaeoclimatol. Palaeoecol.*, *33*(1–3), 205–220, doi:10.1016/0031-0182(81)90039-0.

Bickert, T., and A. Mackensen (2004), Last Glacial to Holocene changes in South Atlantic deep water circulation, in *The South Atlantic in the Late Quaternary: Reconstruction of Material Budgets and Current Systems*, edited by G. Wefer, S. Mulitza, and V. Ratmeyer, pp. 671–695, Springer, Berlin.

Boyle, E. A., and L. D. Keigwin (1987), North Atlantic thermohaline circulation during the past 20,000 years linked to high-latitude surface temperature, *Nature*, *330*(6143), 35–40, doi:10.1038/330035a0.

Broecker, W. S., and E. Maier-Reimer (1992), The influence of air and sea exchange on the carbon isotope distribution in the sea, *Global Biogeochem. Cycles*, *6*, 315–320, doi:10.1029/92GB01672.

Butzin, M., M. Prange, and G. Lohmann (2005), Radiocarbon simulations for the glacial ocean: The effects of wind stress, Southern Ocean sea ice and Heinrich events, *Earth Planet. Sci. Lett.*, *235*(1–2), 45–61, doi:10.1016/j.epsl.2005.03.003.

Clark, P. U., A. S. Dyke, J. D. Shakun, A. E. Carlson, J. Clark, B. Wohlfarth, J. X. Mitrovica, S. W. Hostetler, and A. M. McCabe (2009), The Last Glacial Maximum. *Science*, *325*(5941), 710–714, doi:10.1126/science.1172873.

CLIMAP Project Members (1981), Seasonal reconstruction of the Earth's surface at the Last Glacial Maximum, *Geol. Soc. Am. Map Chart Ser. MC-36*, Geol. Soc. of Am., Boulder, Colo.

Curry, W. B., and D. W. Oppo (2005), Glacial water mass geometry and the distribution of $\delta^{13}C$ of ΣCO_2 in the western Atlantic Ocean, *Paleoceanography*, *20*, PA1017, doi:10.1029/2004PA001021.

Duplessy, J. C., N. J. Shackleton, R. G. Fairbanks, L. Labeyrie, D. W. Oppo, and N. Kallel (1988), Deepwater source variations during the last climatic cycle and their impact on the global deepwater circulation, *Paleoceanography*, *3*, 343–60, doi:10.1029/PA003i003p00343.

England, M. H., and E. Maier-Reimer (2001), Using chemical tracers to assess ocean models. *Rev. Geophys.*, *39*, 29–70.

Fairbanks, R. G. (1989), A 17,000-year glacio-eustatic sea-level record: Influence of glacial melting rates on the Younger Dryas event and deep ocean circulation, *Nature*, *342*(6250), 637–642, doi:10.1038/342637a0.

Fichefet, T., S. Hovine, and J. C. Duplessy (1994), A model study of the Atlantic thermohaline circulation during the Last Glacial Maximum, *Nature*, *372*(6503), 252–255, doi:10.1038/372252a0.

Gersonde, R., et al. (2003), Last glacial sea surface temperatures and sea-ice extent in the Southern Ocean (Atlantic-Indian sector): A multiproxy approach, *Paleoceanography*, *18*(3), 1061, doi:10.1029/2002PA000809.

Gersonde, R., X. Crosta, A. Abelmann, and L. Armand (2005), Sea-surface temperature and sea ice distribution of the Southern Ocean at the EPILOG Last Glacial Maximum—A circum-Antarctic view based on siliceous microfossil records, *Quat. Sci. Rev.*, *24*(7–9), 869–896, doi:10.1016/j.quascirev.2004.07.015.

Hall, I. R., H. K. Evans, D. J. R. Thornalley (2011), Deep water flow speed and surface ocean changes in the subtropical North Atlantic during the last deglaciation, *Global Planet. Change*, doi:10.1016/j.gloplacha.2010.12.001, in press.

Heinze, C., and E. Maier-Reimer (1999), The Hamburg Oceanic Carbon Cycle Model Version "HAMOCC2s" for long time integrations, *Tech. Rep. 20*, Max Planck Inst. fur Meteorol., Hamburg, Germany.

Heinze, C., E. Maier-Reimer, A. M. E. Winguth, and D. Archer (1999), A global oceanic sediment model for long-term climate studies, *Global Biogeochem. Cycles*, *13*, 221–250, doi:10.1029/98GB02812.

Hewitt, C. D., R. J. Stouffer, A. J. Broccoli, J. F. B. Mitchell, and P. J. Valdes (2003), The effect of ocean dynamics in a coupled GCM simulation of the Last Glacial Maximum, *Clim. Dyn.*, *20*(2–3), 203–218, doi:10.1007/s00382-002-0272-6.

Hodell, D. A., J. H. Curtis, F. J. Sierro, and M. E. Raymo (2001), Correlation of late Miocene to early Pliocene sequences between the Mediterranean and North Atlantic, *Paleoceanography*, *16*, 164–178, doi:10.1029/1999PA000487.

Hodell, D. A., K. A. Venz, C. D. Charles, and U. S. Ninnemann (2003), Pleistocene vertical carbon isotope and carbonate gradients in the South Atlantic sector of the Southern Ocean, *Geochem. Geophys. Geosyst.*, *4*(1), 1004, doi:10.1029/2002GC000367.

Kageyama, M., J. Mignot, D. Swingedouw, C. Marzin, R. Alkama, and O. Marti (2009), Glacial climate sensitivity to different states of the Atlantic Meridional Overturning Circulation: results from the IPSL model, *Clim. Past*, *5*(3), 551–570, doi:10.5194/cp-5-551-2009.

Keigwin, L. D. (2004), Radiocarbon and stable isotope constraints on Last Glacial Maximum and Younger Dryas ventilation in the western North Atlantic, *Paleoceanography*, *19*, 15, PA4012, doi:10.1029/2004PA001029.

Key, R. M., A. Kozyr, C. L. Sabine, K. Lee, R. Wanninkhof, J. L. Bullister, R. A. Feely, F. J. Millero, C. Mordy, and T. H. Peng (2004), A global ocean carbon climatology: Results from Global Data Analysis Project (GLODAP), *Global Biogeochem. Cycles*, *18*, GB4031, doi:10.1029/2004GB002247.

Kroopnick, P. M. (1985), The distribution of ^{13}C of ΣCO_2 in the world oceans, *Deep Sea Res., Part A*, *32*(1), 57–84, doi:10.1016/0198-0149(85)90017-2.

Ledbetter, M. T., and D. A. Johnson (1976), Increased transport of Antarctic Bottom Water in Vema Channel during the Last Ice Age, *Science*, *194*(4267), 837–839.

Lohmann, G. (1998), The influence of a near-bottom transport parameterization on the sensitivity of the thermohaline circulation, *J. Phys. Oceanogr.*, *28*(10), 2095–2103.

Lohmann, G., and S. Lorenz (2000), On the hydrological cycle under paleoclimatic conditions as derived from AGCM simulations, *J. Geophys. Res.*, *105*, 17,417–17,436, doi:10.1029/2000JD900189.

Lohmann, G., and M. Schulz (2000), Reconciling Bølling warmth with peak deglacial meltwater discharge, *Paleoceanography*, *15*, 537–540, doi:10.1029/1999PA000471.

Lutze, G. F., and H. Thiel (1989), Epibenthic foraminifera from elevated microhabitats: *Cibicidoides wuellerstorfi* and *Planulina ariminensis*, *J. Foraminif. Res.*, *19*(2), 153–158, doi:10.2113/gsjfr.19.2.153.

Lynch-Stieglitz, J., T. F. Stocker, W. S. Broecker, and R. G. Fairbanks (1995), The influence of air-sea exchange on the isotopic composition of oceanic carbon: Observations and modeling, *Global Biogeochem. Cycles*, *9*(4), 653–665, doi:10.1029/95GB02574.

Lynch-Stieglitz, J., et al. (2007), Atlantic meridional overturning circulation during the Last Glacial Maximum, *Science*, *316*(5821), 66–69, doi:10.1126/science.1137127.

Mackensen, A. (2008), On the use of benthic foraminiferal $\delta^{13}C$ in palaeoceanography: Constraints from primary proxy relationships, in *Biogeochemical Controls on Palaeoceanographic Environmental Proxies*, vol. 303, edited by W. E. N. Austin and R. H. James, *Geol. Soc. Spec. Publ.*, *303*, 121–133, doi:10.1144/SP303.9.

Mackensen, A., H. W. Hubberten, T. Bickert, G. Fischer, and D. K. Futterer (1993), The $\delta^{13}C$ in benthic foraminiferal tests of *Fontbotia wuellerstorfi* (Schwager) relative to the $\delta^{13}C$ of dissolved inorganic carbon in Southern Ocean deep-water: Implications for glacial ocean circulation models, *Paleoceanography*, *8*, 587–610, doi:10.1029/93PA01291.

Mackensen, A., H. Grobe, H. W. Hubberten, and G. Kuhn (1994), Benthic foraminiferal assemblages and the $\delta^{13}C$ signal in the Atlantic sector of the Southern Ocean: Glacial-to-interglacial contrasts, in *Carbon Cycling in the Glacial Ocean: Constraints on the Ocean's Role in Global Change*, *NATO ASI Ser., Ser. I*, vol. 17, edited by R. Zahn et al., pp. 105–144, Springer, New York.

Mackensen, A., H. W. Hubberten, N. Scheele, and R. Schlitzer (1996), Decoupling of $\delta^{13}C_{\Sigma CO2}$ and phosphate in recent Weddell Sea deep and bottom water: Implications for glacial Southern Ocean paleoceanography, *Paleoceanography*, *11*, 203–215, doi:10.1029/95PA03840.

Maier-Reimer, E., U. Mikolajewicz, and K. Hasselmann (1993), Mean circulation of the Hamburg LSG OGCM and its sensitivity to the thermohaline surface forcing, *J. Phys. Oceanogr.*, *23*(4), 731–757.

Marchal, O., and W. B. Curry (2008), On the abyssal circulation in the glacial Atlantic, *J. Phys. Oceanogr.*, *38*(9), 2014–2037, doi:10.1175/2008JPO3895.1.

Meissner, K. J., A. Schmittner, A. J. Weaver, and J. F. Adkins (2003), Ventilation of the North Atlantic Ocean during the Last Glacial Maximum: A comparison between simulated and observed radiocarbon ages, *Paleoceanography*, *18*(2), 1023, doi:10.1029/2002PA000762.

Mix, A. C., E. Bard, and R. Schneider (2001), Environmental processes of the ice age: Land, oceans, glaciers (EPILOG), *Quat. Sci. Rev.*, *20*(4), 627–657, doi:10.1016/S0277-3791(00)00145-1.

Mollenhauer, G., R. R. Schneider, P. J. Muller, V. Spiess, and G. Wefer (2002), Glacial/interglacial variablity in the Benguela upwelling system: Spatial distribution and budgets of organic carbon accumulation, *Global Biogeochem. Cycles*, *16*(4), 1134, doi:10.1029/2001GB001488.

Negre, C., R. Zahn, A. L. Thomas, P. Masque, G. M. Henderson, G. Martinez-Mendez, I. R. Hall, and J. L. Mas (2010), Reversed flow of Atlantic deep water during the Last Glacial Maximum, *Nature*, *468*(7320), 84–88, doi:10.1038/nature09508.

Ninnemann, U. S., and C. D. Charles (2002), Changes in the mode of Southern Ocean circulation over the last glacial cycle revealed by foraminiferal stable isotopic variability, *Earth Planet. Sci. Lett.*, *201*(2), 383–396, doi:10.1016/S0012-821X(02)00708-2.

Olsen, A., and U. Ninnemann (2010), Large δ^{13}C gradients in the preindustrial North Atlantic revealed, *Science*, *330*(6004), 658–659, doi:10.1126/science.1193769.

Oppo, D. W., J. F. McManus, and J. L. Cullen (2003), Deepwater variability in the Holocene epoch, *Nature*, *423*(6938), 400, doi:10.1038/422277b.

Otto-Bliesner, B. L., and E. C. Brady (2010), The sensitivity of the climate response to the magnitude and location of freshwater forcing: Last glacial maximum experiments, *Quat. Sci. Rev.*, *29*(1–2), 56–73, doi:10.1016/j.quascirev.2009.07.004.

Otto-Bliesner, B. L., C. D. Hewitt, T. M. Marchitto, E. Brady, A. Abe-Ouchi, M. Crucifix, S. Murakami, and S. L. Weber (2007), Last Glacial Maximum ocean thermohaline circulation: PMIP2 model intercomparisons and data constraints, *Geophys. Res. Lett.*, *34*, L12706, doi:10.1029/2007GL029475.

Paul, A., and C. Schäfer-Neth (2003), Modeling the water masses of the Atlantic Ocean at the Last Glacial Maximum, *Paleoceanography*, *18*(3), 1058, doi:10.1029/2002PA000783.

Pierre, C., J. F. Saliege, M. J. Urrutiaguer, and J. Giraudeau (2001), Stable isotope record of the last 500 k.y. at Site 1087 (Southern Cape Basin), in *Benguela Current*, edited by G. Wefer, W. H. Berger, and C. Richter, *Proc. Ocean Drill. Program Sci. Results*, *175*, 1–22.

Prange, M., G. Lohmann, and A. Paul (2003), Influence of vertical mixing on the thermohaline hysteresis: Analyses of an OGCM, *J. Phys. Oceanogr.*, *33*, 1707–1721.

Prange, M., G. Lohmann, V. Romanova, and M. Butzin (2004), Modelling tempo-spatial signatures of Heinrich Events: Influence of the climatic background state, *Quat. Sci. Rev.*, *23*, 521–527, doi:10.1016/j.quascirev.2003.11.004.

Rahmstorf, S., and J. Willebrand (1995), The role of temperature feedback in stabilizing the thermohaline circulation, *J. Phys. Oceanogr.*, *25*(5), 787–805.

Robinson, L. F., J. F. Adkins, L. D. Keigwin, J. Southon, D. P. Fernandez, S. L. Wang, and D. S. Scheirer (2005), Radiocarbon variability in the western North Atlantic during the last deglaciation, *Science*, *310*(5753), 1469–1473, doi:10.1126/science.1114832.

Roche, D. M., T. M. Dokken, H. Goosse, H. Renssen, and S. L. Weber (2007), Climate of the Last Glacial Maximum: sensitivity studies and model-data comparison with the LOVECLIM coupled model, *Clim. Past*, *3*(2), 205–224, doi:10.5194/cp-3-205-2007.

Romanova, V., M. Prange, G. Lohmann (2004), Stability of the glacial thermohaline circulation and its dependence on the background hydrological cycle, *Clim. Dyn.*, *22*(5), 527–538, doi:10.1007/s00382-004-0395-z.

Sabine, C. L., R. M. Key, A. Kozyr, R. A. Feely, R. Wanninkhof, F. J. Millero, T. H. Peng, J. L. Bullister, and L. Kitack (2005), Global Ocean Data Analysis Project (GLODAP): Results and data, *Tech. Rep. ORNL/CDIAC-145, NDP-083*, Carbon Dioxide Inf. Anal. Cent., Oak Ridge Natl. Lab., Oak Ridge, Tenn.

Sarnthein, M., K. Winn, S. J. A. Jung, J. C. Duplessy, L. Labeyrie, H. Erlenkeuser, and G. Ganssen (1994), Changes in east Atlantic deepwater circulation over the last 30,000 years: Eight time slice reconstructions, *Paleoceanography*, *9*, 209–267, doi:10.1029/93PA03301.

Sarnthein, M., R. Gersonde, S. Niebler, U. Pflaumann, R. Spielhagen, J. Thiede, G. Wefer, and M. Weinelt (2003), Overview of Glacial Atlantic Ocean Mapping (GLAMAP 2000), *Paleoceanography*, *18*(2), 1030, doi:10.1029/2002PA000769.

Schäfer-Neth, C., and A. Paul (2001), Circulation of the glacial Atlantic: A synthesis of global and regional modeling, in *The Northern North Atlantic: A Changing Environment*, edited by P. Schäfer et al., pp. 441–462, Springer, Berlin.

Schmittner, A. (2003), Southern Ocean sea ice and radiocarbon ages of glacial bottom waters, *Earth Planet. Sci. Lett.*, *213*(1–2), 53–62, doi:10.1016/S0012-821X(03)00291-7.

Seidov, D., E. Barron, and B. J. Haupt (2001), Meltwater and the global ocean conveyor: Northern versus southern connections, *Global Planet. Change*, *30*(3–4), 257–270.

Shin, S. I., Z. Liu, B. L. Otto-Bliesner, E. C. Brady, J. E. Kutzbach, and S. P. Harrison (2003a), A simulation of the Last Glacial Maximum climate using the NCAR-CCSM, *Clim. Dyn.*, *20*(2–3), 127–151, doi:10.1007/s00382-002-0260-x.

Shin, S. I., Z. G. Liu, B. L. Otto-Bliesner, J. E. Kutzbach, and S. J. Vavrus (2003b), Southern Ocean sea-ice control of the glacial North Atlantic thermohaline circulation, *Geophys. Res. Lett.*, *30*(2), 1096, doi:10.1029/2002GL015513.

Slowey, N. C., and W. B. Curry (1995), Glacial-interglacial differences in circulation and carbon cycling within the upper western North Atlantic, *Paleoceanography*, *10*, 715–732, doi:10.1029/95PA01166.

Stocker, T. F., D. G. Wright, and W. S. Broecker (1992), The influence of high-latitude surface forcing on the global thermohaline circulation, *Paleoceanography*, *7*, 529–541, doi:10.1029/92PA01695.

Tagliabue, A., L. Bopp, D. M. Roche, N. Bouttes, J. C. Dutay, R. Alkama, M. Kageyama, E. Michel, and D. Paillard (2009), Quantifying the roles of ocean circulation and biogeochemistry in governing ocean carbon-13 and atmospheric carbon dioxide at the Last Glacial Maximum, *Clim. Past*, *5*(4), 695–706, doi:10.5194/cp-5-695-2009.

Taylor, K. E. (2001), Summarizing multiple aspects of model performance in a single diagram, *J. Geophys. Res.*, *106*, 7183–7192, doi:10.1029/2000JD900719.

Weber, S. L., S. S. Drijfhout, A. Abe-Ouchi, M. Crucifix, M. Eby, A. Ganopolski, S. Murakami, B. L. Otto-Bliesner, and W. R. Peltier (2007), The modern and glacial overturning circulation in the Atlantic Ocean in PMIP coupled model simulations, *Clim. Past*, *3*(1), 51–64, doi:10.5194/cp-3-51-2007.

Winguth, A. M. E., D. Archer, J. C. Duplessy, E. Maier-Reimer, and U. Mikolajewicz (1999), Sensitivity of paleonutrient tracer distributions and deep-sea circulation to glacial boundary conditions, *Paleoceanography*, *14*, 304–323, doi:10.1029/1999PA900002.

Woodruff, F., S. M. Savin, and R. G. Douglas (1980), Biological fractionation of oxygen and carbon isotopes by recent benthic foraminifera, *Mar. Micropaleont.*, *5*(1), 3–11, doi:10.1016/0377-8398(80)90003-1.

Yu, J. M., H. Elderfield, and A. M. Piotrowski (2008), Seawater carbonate ion-δ^{13}C systematics and application to glacial-interglacial North Atlantic ocean circulation, *Earth Planet. Sci. Lett.*, *271*(1–4), 209–220, doi:10.1016/j.epsl.2008.04.010.

Zahn, R., and R. Keir (1994), Tracer-nutrient correlations in the upper ocean: Observational and box model constraints on the use of benthic foraminiferal δ^{13}C and Cd/Ca as paleo-proxies for the intermediate-depth ocean, in *Carbon Cycling in the Glacial Ocean: Constraints on the Ocean's Role in Global Change*, *NATO ASI Ser., Ser. I*, vol. 17, edited by R. Zahn et al., pp. 195–221, Springer, New York.

Zahn, R., K. Winn, and M. Sarnthein (1986), Benthic foraminiferal δ^{13}C and accumulation rates of organic carbon: *Uvigerina peregrina* group and *Cibicidoides wuellerstorfi*, *Paleoceanography*, *1*, 27–42, doi:10.1029/PA001i001p00027.

Zahn, R., M. Sarnthein, and H. Erlenkeuser (1987), Benthic isotope evidence for changes of the Mediterranean outflow during the Late Quaternary, *Paleoceanography*, *2*, 543–559, doi:10.1029/PA002i006p00543.

T. Bickert and M. Butzin, MARUM–Center for Marine Environmental Sciences, D-28334 Bremen, Germany. (tbickert@marum.de; mbutzin@marum.de)

T. Hesse and G. Lohmann, Alfred Wegener Institute for Polar and Marine Research, Bussestr. 24, D-27570 Bremerhaven, Germany. (tilman.hesse@awi.de; gerrit.lohmann@awi.de)